

Metal-Organic Framework-Based Electrodes for Asymmetric Supercapacitors

Liuli Zhang,^[a, b] Yisong Wang,^[c] Cui Yang,^{*[a]} and Kai Tao^{*[b]}

Supercapacitors (SCs) are a promising electrochemical device in the field of electrochemical energy storage, but their wide range applications are limited by relatively low energy density. Asymmetric supercapacitors (ASCs) based on different positive and negative electrodes offer the possibility to increase the energy density by extending the voltage window. It is essential to explore novel electrode materials to boost the electrochemical properties of ASCs. Metal-organic frameworks (MOFs) have emerged as ideal electrode materials for SCs, due to their high porosity, tunable structure and highly dispersed active

sites. MOFs can also be used as templates or precursors for the preparation of versatile electrode materials, such as carbon materials and metal compounds. In this minireview, SCs and MOF-based electrode materials are first introduced, followed by an overview of recent advances in the synthesis of MOF-based electrode materials including pristine MOFs, MOF derivatives and their composites, and their applications in ASCs acted as negative electrode, positive electrode or both. Finally, the challenges and prospects of MOF-based ASCs are discussed.

1. Introduction

In recent years, the increasing energy demand and the environmental pollution caused by drastic consumption of fossil energy, and the uneven and limited distribution of resources have prompted the development and advancement of advanced energy storage technologies.^[1–5] In this regard, sustainable electrochemical energy conversion and storage technologies, such as lithium-ion batteries (LIBs), potassium-ion batteries (PIBs), supercapacitors (SCs), fuel cells and metal-air batteries have been intensively explored.^[6–10] SCs have attracted particular interest in portable and wearable electronic devices owing to their high power density, fast charging and discharging, excellent cycling stability, lightweight and compact size, and no pollution to the environment.^[11–14] However, the critical issue of SCs is the relatively low energy density, which prevents the development of their practical applications.^[15] SCs typically consist of two electrodes (negative and positive) in electrolyte (aqueous or organic solvent), and separated by a separator that allows for ions transport while maintaining electrical insulation between two electrodes.^[16] The electrode materials play a crucial role in determining electrochemical performance of SCs, and they are divided into capacitive (carbon materials), pseudocapacitive (MnO_2 , Fe_2O_3 , MoO_3) and battery-like (Co_3O_4 , NiO , Co_3S_4) types based on different charge storage mechanisms.^[17] Depending on the different active materials of

positive and negative electrodes, SCs can be roughly classified into symmetric supercapacitors, asymmetric supercapacitors (ASCs) and/or hybrid supercapacitors.^[18] The energy density of SCs is related to the operating voltage window (V) and the capacitance (C) of the device as described by following equation:^[19]

$$E = CV^2/2 \quad (1)$$

Thus, fabrication of ASCs has become a very effective strategy to increase the energy density by coupling the different potential windows of the two different electrodes during charging and discharging to maximize the operating voltage of the whole device.^[20] In addition, ASCs have a distinct advantage in energy storage systems, because they can combine high energy density of batteries with the fast charge/discharge rates of conventional SCs.^[21] However, ASCs currently suffer from unsatisfactory positive and negative electrode materials, and the mismatch between two electrodes.^[22,23] Therefore, great efforts have been made to exploring electrode materials with desirable morphology, high porosity and good electronic conductivity to maximize the electrochemical performance of ASCs.^[24]

As a kind of coordination polymers, metal-organic frameworks (MOFs) composed of organic linkers (usually containing imidazolates/carboxylates or groups) and metal centers (ions/clusters) have received wide attention in many fields such as energy storage, catalysis and sensors owing to the characteristics of controllable structure, tuneable pore size, large achievable surface area, and permeability to guest molecules.^[25–27] To present, more than 20,000 MOFs have been synthesized by selecting different metal centers and organic linkers.^[28] MOFs usually possess a higher specific surface area and a more ordered pore structure than conventional microporous and mesoporous materials, which endows MOFs with great potential for application as electrode materials of

[a] L. Zhang, C. Yang
Institute of Drug Discovery Technology, Ningbo University, Ningbo, Zhejiang, 315211, China
E-mail: yangcui@nbu.edu.cn

[b] L. Zhang, Dr. K. Tao
School of Materials Science & Chemical Engineering, Ningbo University, Ningbo, Zhejiang 315211, China
E-mail: taokai@nbu.edu.cn

[c] Y. Wang
Taizhou Technician College, Taizhou 318000, China

SCs.^[26,29,30] Besides, the multiple oxidation states of metal ions enable rich redox reactions and high capacity. Nevertheless, the poor electronic conductivity and structural instability of most MOFs hampers their utilizations.^[31] To solve these problems, many effective strategies have been employed, such as designing conductive MOFs through coordination chemistry and coupling with carbon materials. Alternatively, the intrinsic defects of MOFs can be resolved by converting MOFs into porous carbon, metal oxides/hydroxides, metal sulfides, etc., where the morphology and porosity of MOF templates can be roughly retained. Therefore, MOF-based materials including pristine MOFs, MOF derivatives and their composites have emerged as potential electrodes for SCs.^[32,33]

There are several insightful reviews on MOF-based electrode materials, focusing on the different categories and micro-nanostructures of MOFs, and their electrochemical performances in three-electrode systems.^[34,35] Given that the two-electrode cell performance is more indicative for real applications, and a growing number of ASCs assembled from MOF-based electrode materials have been reported during the last few years, it is urgent to review the advances. This article presents an overview of MOF-based materials including pristine MOFs, MOF derivatives and their composites used as electrodes (negative, positive and both) of ASCs. Table 1 presents the representative research results of MOF-based electrode materials for ASCs. The current limitation, challenges and development prospects of MOF-based electrode materials, and their assembled ASCs are discussed.

2. MOF-Based Materials as Electrodes for ASC Devices

2.1. Negative Electrodes

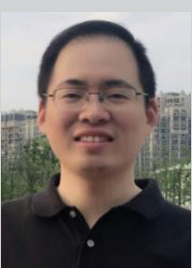
Activated carbon (AC) is one of the mostly used negative electrode materials for ASCs. However, its low specific capacitance results in inferior energy density of ASCs. Thus, there is an urgent need for new negative electrode materials with high capacitance and good stability. Recently, MOFs have been explored for energy storage because the highly ordered pore structure can accommodate the electrolyte.^[66] However, MOFs are seldom used as negative active components. Ding et al.

successfully synthesized hierarchical MOF nanosheets (EV-HNSs) self-assembled from negatively electroactive organic viologen ligands and europium ions, and used them as negative electrodes for ASCs.^[36] Using MnO₂ as the positive electrode, the prepared MnO₂/EV-HNSs ASC achieved a good working voltage (1.55 V) and high areal energy density (9.4 $\mu\text{Wh cm}^{-2}$ at 775 $\mu\text{W cm}^{-2}$), which was better than many reported ASCs devices. Wang et al. conducted a preliminary exploration of polyoxometalate-based metal-organic frameworks (POMOFs) as negative electrode materials for ASCs by depositing Fe-VO₄-BIPY on the surface of graphene oxide (GO) to enhance the electrical conductivity and dispersion of Fe-VO₄-BIPY.^[37] When, it was assembled with the positive Ni(OH)₂ electrode, the ASC device delivered the maximum energy density of 46.84 Wh kg⁻¹.

Most MOFs are insulated and unstable in electrolyte. Fortunately, MOFs can be used as self-sacrificing templates to prepare porous carbons by annealing MOFs under inert atmospheres. The MOF-derived carbon materials display high specific surface, tuneable microstructure and good electronic conductivity, which are beneficial for enhancing electrochemical performance of SCs.^[67] Kim et al. prepared porous carbon (MDC-A) from a single Fe-MOF (MIL-100 (Fe)), which had a large surface area and high porosity.^[68] Besides, Fe is cheaper and non-toxic compared to other metals (e.g., Co and Cr). An ASC was assembled with MDC-A as the negative electrode and α -Fe₂O₃ as the positive electrode, and delivered superior energy density (25.5 Wh kg⁻¹) at a power density 60 W kg⁻¹. The specific capacity retention of ASC was 90.11% after 5000 charging and discharging cycles. Bimetallic ZnCo-MOF was also employed to prepare nanoporous carbon polyhedron (NPC) by Javed et al.^[39] The flexible ASC with Zn-Co-O@CC as the positive electrode and NPC@CC as the negative electrode could work at a high voltage window of 2.0 V, and displayed outstanding energy storage performance (117.9 Wh kg⁻¹ at 1490.4 W kg⁻¹). The heteroatoms (e.g., S and N) in the organic ligands of MOFs can be doped in carbon framework during pyrolysis, which boosts the capacitance (capacitive and pseudocapacitive) of carbon materials. Nitrogen-doped nanoporous carbon nanosheets (NPC) were obtained by annealing ZnCo-ZIF, where the imidazole linker contained a large content of N.^[40] An ASC was assembled by using binder-free NiCo₂O₄ ultrathin nanosheets supported on carbon fiber paper (Ni-Co-O@CFP) as the positive electrode and NPC as the negative electrode. The ASC exhibited a high energy density of 69 Wh kg⁻¹ (840 W kg⁻¹) and



Liulu Zhang was born in 1999, Anhui Province, China. She is now an M.S. candidate under the supervision of Prof. Kai Tao at the School of Materials Science and Chemical Engineering, Ningbo University, China. Her thesis focuses on the synthesis of MOF-derived nanostructures and their applications in supercapacitors and alkaline batteries.



Dr. Kai Tao received his PhD degree from Toyama University (Japan) in 2012 under the supervision of Prof. Noritatsu Tsubaki. Then, he worked in the group of Prof. Liang Chen at the Ningbo Institute of Materials Technology and Engineering, Chinese Academy of Sciences (CAS). Currently, he is a Professor at the School of Materials Science and Chemical Engineering, Ningbo University. His research interest is in the development of porous functional materials for applications in catalysis and energy storage.

Table 1. Representative MOF-based electrode materials for ASCs.

MOF	MOF-based electrode	ASC	Voltage window	Energy density	Ref.
Negative electrode					
EV-HNSs	EV-HNSs	MnO ₂ //EV-HNSs	1.55 V	9.4 µWh cm ⁻²	[36]
Fe-VO ₄ -BIPY	GO/Fe-VO ₄ -BIPY	Ni(OH) ₂ //GO/Fe-VO ₄ -BIPY	1.6 V	46.84 Wh kg ⁻¹	[37]
ZIF-67	CNT@HCNF-1.5	Co ₃ O ₄ @NF//CNT@HCNF-1.5	1.6 V	87.5 Wh kg ⁻¹	[38]
ZnCo-MOF	NPC	Zn–Co–O//NPC	2 V	117.9 Wh kg ⁻¹	[39]
ZIF-8/ZIF-67	NPC	Ni–Co–O//NPC	1.8 V	69 Wh kg ⁻¹	[40]
Fe-MOF	α-Fe ₂ O ₃	AC//α-Fe ₂ O ₃	1.8 V	63 Wh kg ⁻¹	[41]
Fe-MOF	Fe ₂ O ₃ @C/rGO	NiCo ₂ O ₄ //Fe ₂ O ₃ @C/rGO	1.7 V	101.9 Wh kg ⁻¹	[42]
Bi-MOF	Bi ₂ O ₃	CoNiMn-LDH//Bi ₂ O ₃	1.5 V	120 Wh kg ⁻¹	[43]
Mn-BTC	Mn ₂ O ₃ /C	Mn ₂ O ₃ /C//AC	1.8 V	54.9 Wh kg ⁻¹	[44]
Positive electrode					
Co-BTB-LB	Co-BTB-LB	Co-BTB-LB//AC	1.6 V	150.2 Wh kg ⁻¹	[45]
NiMn-MOF	NiMn-MOF	NiMn-MOF//AC	1.6 V	55.0 Wh kg ⁻¹	[46]
Ni/Co-MOF	Ni/Co-MOF@TCT-NH ₂	Ni/Co-MOF@TCT-NH ₂ //AC	1.5 V	98.1 Wh kg ⁻¹	[47]
Ni-MOF	NiO/Ni-MOF	NiO/Ni-MOF//AC	1.6 V	31.3 Wh kg ⁻¹	[48]
Ni-MOF	NiO/Ni/NCNTs	NiO/Ni/NCNTs//PC	1.6 V	33.9 Wh kg ⁻¹	[49]
Ni–Co BTC	NiCo ₂ O ₄	NiCo ₂ O ₄ //AC	1.6 V	84.3 Wh kg ⁻¹	[50]
ZIF-67	MnCoNi-LDH	MnCoNi-LDH//AC	1.6 V	47.4 Wh kg ⁻¹	[51]
NiCo-ZIF	NCNRs@NCZIFs	NCNRs@NCNSs//AC	1.5 V	22.8 Wh kg ⁻¹	[52]
ZIF-67	r-NiCo ₂ S ₄	r-NiCo ₂ S ₄ //AC	1.6 V	43.8 Wh kg ⁻¹	[53]
Fe-MOF	Fe-MoS ₂	Fe-MoS ₂ //O, N, S@AC	1.6 V	49.4 Wh kg ⁻¹	[54]
ZIF-67	NiCoMn-S	NiCoMn-S//AC	1.7 V	50.0 Wh kg ⁻¹	[55]
ZnCo-ZIF	Zn _{0.33} Co _{0.67} P	Zn _{0.33} Co _{0.67} P//Bi ₂ O ₃	1.7 V	83.1 Wh kg ⁻¹	[56]
ZnNi-MOF	ZnNiP	ZnNiP//rGO	1.6 V	67.4 Wh kg ⁻¹	[57]
NiFe-PBA	Ni–Fe–Mn–Se	Ni–Fe–Mn–Se//AC	1.6 V	66.8 Wh kg ⁻¹	[58]
CoFe-PBA	(CoFe)Se ₂ @NC	(CoFe)Se ₂ @NC//Fe ₂ O ₃ /rGO	1.5 V	20 Wh kg ⁻¹	[59]
Positive and negative electrode					
FeSC	(+) FeSC (-) FeSC#	FeSC//FeSC#	1.6 V	49.9 Wh kg ⁻¹	[60]
ZIF-8	(+) ZnO QD/NPC/CNF (-) NPC/CNF	ZnO QD/NPC/CNF//NPC/CNF	1.6 V	33.8 Wh kg ⁻¹	[61]
Zn/Co-ZIF	(+) ZnCo ₂ O ₄ (-) NPC	ZnCo ₂ O ₄ //NPC	1.45 V	28.6 Wh kg ⁻¹	[62]
Co-TAMBA-d and Fe-TAMBA-d	(+) Co-TAMBA-d (-) Fe-TAMBA-d	Co-TAMBA-d//Fe-TAMBA-d	1.5 V	47 Wh kg ⁻¹	[63]
ZIF	(+) ZnNiCo-LDH/CuO–Cu (-) N-CNT	ZnNiCo-LDH/CuO–Cu//N-CNT	1.6 V	117.5 Wh kg ⁻¹	[64]
POMOF	(+) NENU-5/PPy (-) FeMo/C	NENU-5/PPy// FeMo/C	1 V	1.1 mWh cm ⁻³	[65]

excellent cycling durability, maintaining more than 90% capacitance over 20,000 cycles. Kim et al. used an *in situ* developed of MOF-based thermal treatment to grow highly porous N-doped carbon nanotubes (CNTs) containing submerged Co nanoparticles on nano-fibrillated electrospun hollow carbon nanofibers (HCNFs), as demonstrated by Figure 1a.^[38] The ASC was assembled with Co₃O₄@NF as the positive electrode and CNT@HCNF-1.5 as the negative electrode. The capacity retention rate of ASC reaches 93.2% after 10,000 consecutive charge/discharge cycles (Figure 1b), and the ASC

achieves a high energy density of 87.5 Wh kg⁻¹ at a power density of 799.9 W kg⁻¹ (Figure 1c).

MOFs can also be transformed into porous metal oxides through annealing oxidative atmospheres. Compared with carbon materials, transition metal oxides (TMOs), such as Fe₂O₃, Bi₂O₃ and MnO₂ provide larger capacitance by virtue of rich redox reactions. Therefore, MOF-derived TMOs are suitable negative electrodes for ASCs. For example, an α-Fe₂O₃ nano-octahedron as negative electrode was synthesized by annealing MIL-88 (Fe) at 500 °C in air and N₂ atmospheres for 2 h,

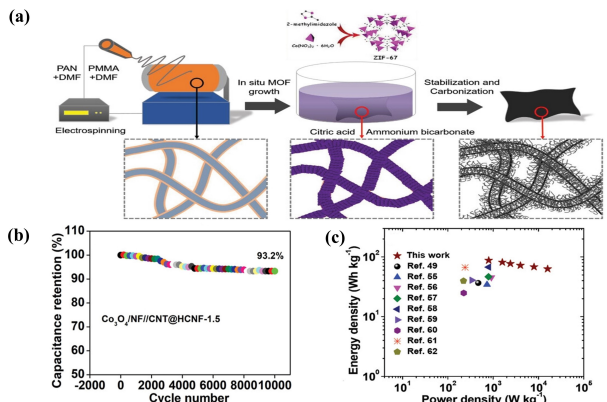


Figure 1. (a) Schematic illustration of the fabrication of the CNT@HCNF-x electrode. (b) Cyclic stability of the $\text{Co}_3\text{O}_4@\text{NF}/\text{CNT}@\text{HCNF}-1.5$ ASC device. (c) Ragone plots for the $\text{Co}_3\text{O}_4@\text{NF}/\text{CNT}@\text{HCNF}-1.5$ ASC device. Reprinted with permission from ref. [38], Copyright 2022, Wiley-VCH.

separatively.^[41] The MOF-derived $\alpha\text{-Fe}_2\text{O}_3$ showed large surface area, and the formation of oxygen vacancies improved the conductivity and accelerated the ionic transport, thereby boosting the electrochemical activity.^[69,70] The electrode provided a high specific capacity of 250.2 mAh g^{-1} at 1 A g^{-1} . When it was coupled with an AC electrode, the resulting ASC offered a high energy density of 63 Wh kg^{-1} with a power density of 900 W kg^{-1} . However, the poor conductivity, sluggish ion diffusion kinetics, and volume expansion of iron oxides result in poor rate capability and cycling stability. To overcome these obstacles, graphene oxide (GO) was used as matrix to grow Fe-MOF with the help of PVP, and the $\text{FeO}_x@\text{C/rGO}$ nanocomposites with different crystalline phase and FeO_x particle sizes could be obtained by calcination at different conditions (Figure 2a).^[42] All the CV curves present distinct redox peaks

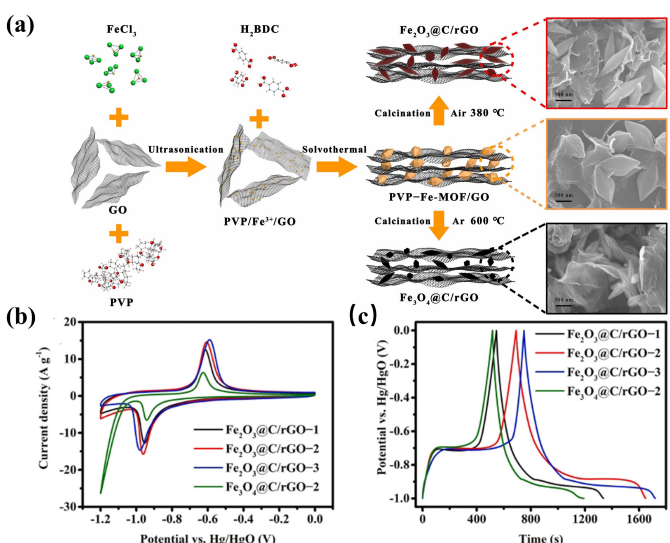
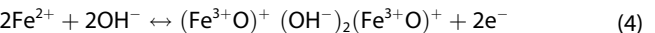
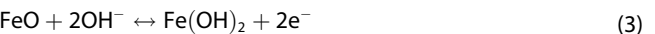
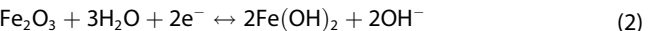


Figure 2. (a) Schematic illustration of the synthetic process for $\text{FeO}_x@\text{C/rGO}$ nanocomposites. (b) CV curves at 10 mV s^{-1} and (c) GCD curves at 1 A g^{-1} for $\text{Fe}_3\text{O}_4@\text{C/rGO}-1$, $\text{Fe}_2\text{O}_3@\text{C/rGO}-2$, $\text{Fe}_2\text{O}_3@\text{C/rGO}-3$ and $\text{Fe}_3\text{O}_4@\text{C/rGO}-2$ electrodes. Reprinted with permission from ref. [42], Copyright 2022, Elsevier.

(Figure 2b). The reason for this is due to the reversible transition between $\text{Fe}^{2+}/\text{Fe}^{3+}$. The possible redox reactions are expressed as follows.^[42,71]



The optimized $\text{Fe}_2\text{O}_3@\text{C/rGO}-2$ nanocomposite exhibited large surface area with Fe_2O_3 nanoparticles (NPs, $< 5 \text{ nm}$) embedded in the carbon matrix, which gave rise to high specific capacitance and remarkable cycle life (Figure 2c). The $\text{Fe}_2\text{O}_3@\text{C/rGO}-2$ and a NiCo_2O_4 electrode were assembled into an ASC, the ASC displays a high specific capacity of 458.3 Cg^{-1} , corresponding to an energy density of 101.9 Wh kg^{-1} . Compared iron oxides, Bi_2O_3 possesses the advantages of high theoretical capacity (385 mAh g^{-1}) and large working potential. Therefore, Bi_2O_3 could be a promising negative electrode for ASCs. Wang et al. reported the synthesis of Bi_2O_3 nanorods by treating Bi-MOF in 1 M KOH solution. The MOF-derived Bi_2O_3 presented highly reversible redox reactions in the voltage range of -1.1 to -0.2 V , and displayed a high specific capacity of 226.1 mAh g^{-1} at 1 A g^{-1} .^[43] When it was matched with a positive electrode (CoNiMn-LDH), the resulting CoNiMn-LDH// Bi_2O_3 ASC achieved a high energy density of 120 Wh kg^{-1} at a power density of 4.2 kW kg^{-1} . Besides, manganese oxides are also widely used as negative electrodes for ASCs. Nagamuthu et al. prepared a porous $\text{Mn}_2\text{O}_3/\text{C}$ composite by calcining Mn-BTC.^[44] The $\text{Mn}_2\text{O}_3/\text{C}$ exhibited high specific capacitance (776 Fg^{-1}) without capacitance loss during the cycling process. The ASC used $\text{Mn}_2\text{O}_3/\text{C}$ as the negative electrode showed a high energy density of 54.9 Wh kg^{-1} at a power density of 2.2 kW kg^{-1} .

Pristine MOFs and their composites are seldom used as negative electrode materials. MOFs can be ideal templates for the synthesis of carbon materials and metal oxides, which have unique nanostructures with highly porosity and multifunction. This is essential for achieving enhanced electrochemical performance, and offers many options for developing new negative materials.

2.2. Positive Electrodes

In recent years, pristine MOFs with desirable pore size and higher surface areas have been explored as positive electrode materials for ASCs because the multiple oxidation states of metal ions enable rich redox reactions and high capacity. For example, Liu et al. synthesized a 2D MOF nanosheets Co-BTB-LB using liquid-liquid interface-assisted method, and the capacity of the Co-BTB-LB electrode was high as 4969.3 Fg^{-1} at 1 A g^{-1} .^[45] The ASC assembled with Co-BTB-LB as the positive electrode and AC as the negative electrode showed good energy storage performance, with a maximum energy density of 150.2 Wh kg^{-1} at a power density of 1619.2 W kg^{-1} . The

capacitance retention after 10,000 cycles at 10 A g^{-1} was 97.1%. In another work, Pallavolu et al. synthesized a bimetallic NiMn-MOF electrode materials using a simple hydrothermal synthesis method, and the NiMn-MOF presents sufficient voids and pores for rapid insertion of electrolyte ions to increase pseudocapacitance.^[46] An ASC assembled with NiMn-MOF as the positive electrode and AC as the negative electrode displayed a high specific capacitance of 160 F g^{-1} , an energy density of 55.0 Wh kg^{-1} at a power density of 785 W kg^{-1} , and a capacitance retention of 94% after 5000 cycles. To overcome the low conductivity and poor stability of pristine MOFs, conductive substances including carbon materials, metal compounds and conductive polymers are usually incorporated to construct MOF-based composites. For example, Yue et al. employed 2D thin-layer aminated $\text{Ti}_3\text{C}_2\text{T}_x$ MXene (denoted as TCT-NH₂) as supporting substance for in situ growth of bimetallic Ni/Co-MOF, as shown in Figure 3a.^[47] Taking the advantages of high redox activity of bimetallic Ni/Co-MOF, and the conductive network with outstanding stability of MXene, the prepared Ni/Co-MOF@TCT-NH₂ composite displayed excellent electrochemical performance as a battery-type electrode (Figure 3b and c). When coupling with an AC electrode, the fabricated ASC cell could exhibit a high energy density of 98.1 Wh kg^{-1} at 600 W kg^{-1} with impressive cycle life (99.3% after 15,600 cycles).

Wang et al. constructed NiO/Ni-MOF nanocomposites by in situ conversion of NiO nanoflakes into Ni-MOF in presence of terephthalic acid (TPA) linker.^[48] In hydrothermal process, TPA readily reacted with the nickel oxide template, releasing Ni²⁺ ions from the NiO precursor. Simultaneously, the formed Ni²⁺ ions coordinated with TPA ligands to produce Ni-MOF over the NiO template. Therefore, the degree conversion of NiO to Ni-MOF could be more easily regulated by the amount of TPA added during the hydrothermal process. The XRD peaks associated with NiO became weaker and the characteristic peaks of Ni-MOF became more pronounced as the TPA content

increased, indicating that the conversion of NiO to Ni-MOF was increasing (Figure 4a). The characteristic FTIR peaks of Ni-MOF became more prominent with the increase of TPA dosage, which further verified the formation of more Ni-MOF in the composites (Figure 4b). The optimized NiO/Ni-MOF-25 displayed higher specific capacity than the other materials (Figure 4c and d). The assembled NiO/Ni-MOF-25//AC could output a maximum energy density of 31.3 Wh kg^{-1} .

Apart from being directly utilized as positive electrode materials for SCs, MOFs have emerged as ideal sacrificial templates/precursors for constructing porous metal oxide/hydroxide, sulfide, phosphate/phosphide and selenide. The MOF derivatives inherit micro-nanostructure and porosity of parent MOFs. Therefore MOF derivatives have attracted great interest in electrochemical energy storage applications.^[72]

Transition metal oxides (TMOs), such as Co_3O_4 and NiO are promising positive electrode materials for SCs due to their high theoretic capacity. MOFs can be converted into TMOs, metals, carbon and their composites simply by adjusting the annealing conditions. Therefore, various TMOs-based electrode materials derived from MOFs have been widely used in SCs. Wang et al. successfully prepared NiO/Ni embedded N-doped carbon nanotubes (NiO/Ni/NCNTs) through two-step calcination of Ni-MOF template, as depicted by Figure 5a.^[49] Under annealing at high temperatures ($500/600/700^\circ\text{C}$) in N_2 atmosphere, Ni²⁺ in Ni-MOF was partially reduced to Ni, which catalyzed the formation of NCNTs. After that, NiO/Ni/NCNTs composites with high NiO content were successfully synthesized using a low-temperature calcination process in air. The NiO/Ni/NCNTs composite not only possessed rich redox sites, but also provided conductive channels for charge transfer. The resulting NiO/Ni/NCNTs composite exhibited a specific capacitance of 777.5 F g^{-1} at 1 A g^{-1} in three-electrode system. An ASC assembled from NiO/Ni/NCNTs and porous carbon could output an energy density of 33.89 Wh kg^{-1} at a power density of 800 W kg^{-1} . More importantly, the ASC device retained 90%

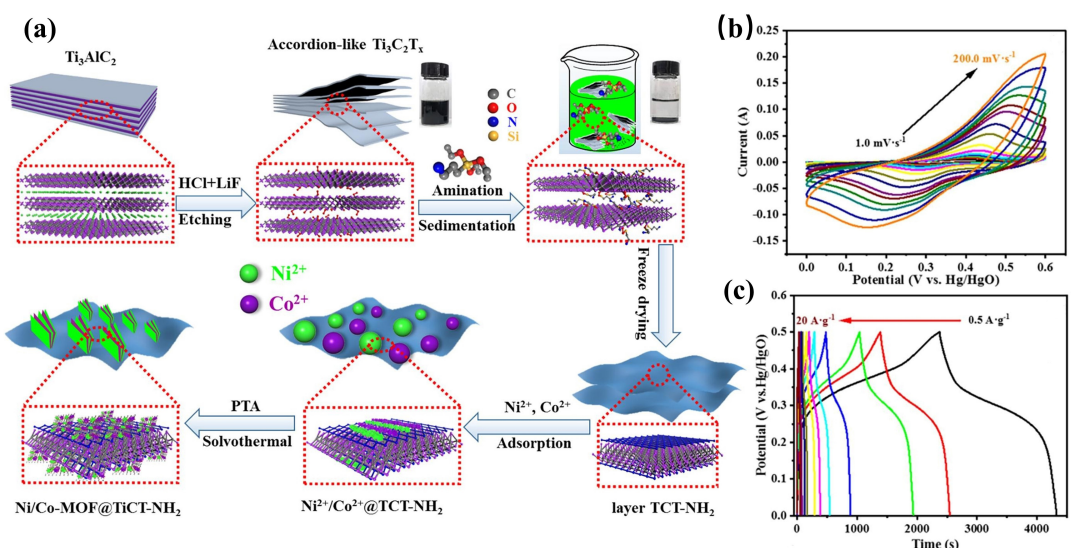


Figure 3. (a) Schematic illustration of the synthesis of Ni/Co-MOF@TCT-NH₂ composite. (b) CV and (c) GCD curves of the Ni/Co-MOF@TCT-NH₂ composite. Reprinted with permission from ref. [47], Copyright 2022, Elsevier.

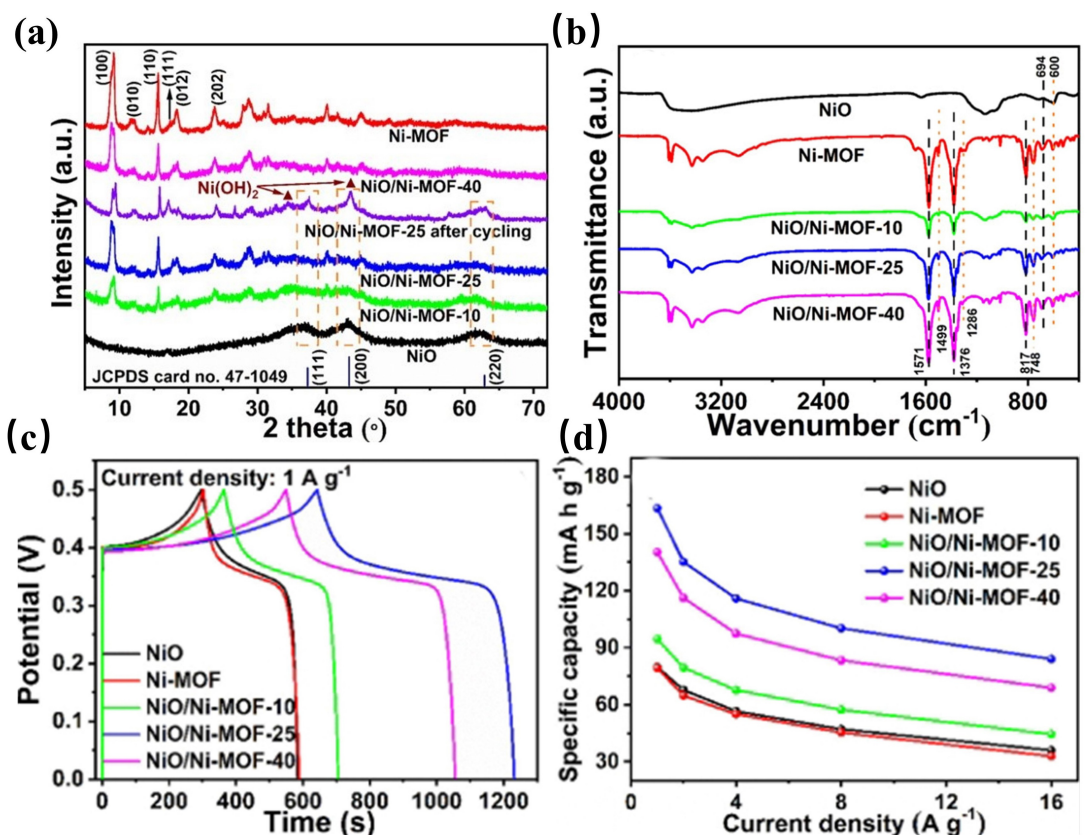


Figure 4. (a) XRD patterns, (b) FTIR spectra, (c) GCD curves and (d) specific capacity for NiO, Ni-MOF and NiO/Ni-MOF composites. Reprinted with permission from ref. [48], Copyright 2021, American Chemical Society.

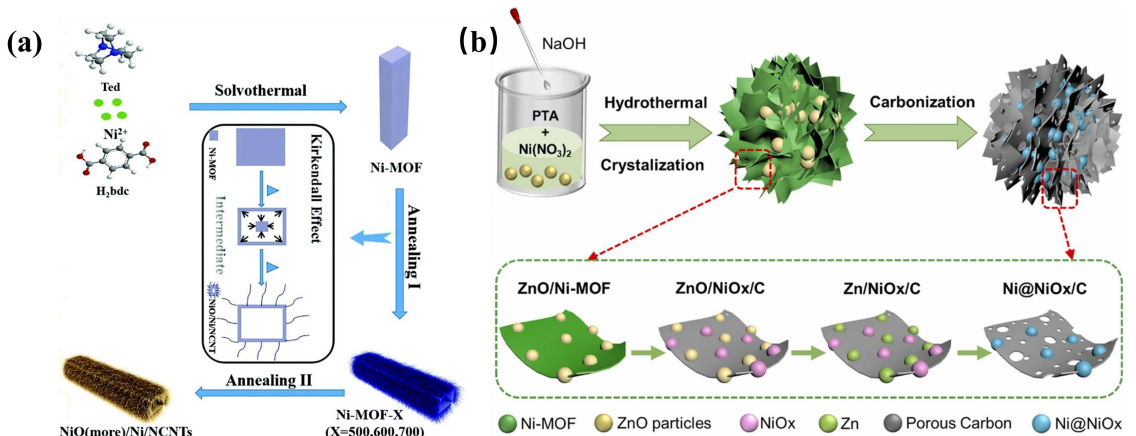


Figure 5. (a) Schematic of the preparation of NiO/Ni/NCNTs. Reprinted with permission from ref. [49], Copyright 2019, Royal Society of Chemistry. (b) Schematic diagram of synthesis of Ni@NiO_x/C nanosheets. Reprinted with permission from ref. [73], Copyright 2022, Elsevier.

initial capacitance after 40 000 cycles, demonstrating impressive cycling durability. Similarly, Ni@NiO_x NPs encapsulated porous carbon nanosheets (Ni@NiO_x/C) were prepared from ZnO NPs embedded Ni-MOF nanosheets (ZnO/Ni-MOF) through controlled thermal treatment (Figure 5b).^[73] The incorporation of ZnO NPs could optimize the morphology and porous structure of the composite. The optimized Ni@NiO_x/C-2 electrode exhibited a specific capacitance of 752 Fg⁻¹ at 1 Ag⁻¹ with

remarkable capacitance retention (99%, after 10,000 cycles). The prepared Ni@NiO_x/C-2//AC could deliver a high power density (15840 W kg⁻¹), but the energy density was moderate. Mixed metal oxides are superior to monometallic oxides due to improved electronic conductivity and charge transfer. Salunkhe et al prepared spinel NiCo₂O₄ nanosheets by annealing bimetallic Ni–Co MOF at different temperatures.^[50] The NiCo₂O₄ annealed at 300 °C exhibited the best electrochemical perform-

ance due to optimized surface area and wettability. In addition, the fabricated NiCo₂O₄//AC ASC displayed excellent energy density 84.26 Wh kg⁻¹ at a power density of 1185 W kg⁻¹.

Metal hydroxides, especially layered double hydroxides (LDHs) represent a significant kind of battery-like electrode materials for SCs. The exchangeable compensated anions and water molecules between the LDH layers ensure abundant redox reactions, and the bimetallic oxides or hydroxides have a variety of oxidation states, resulting in superior electrochemical properties.^[74] MOF-derived LDHs are significant candidates for advanced SCs due to ease synthesis of versatile micro-nanostructures with high electrochemical activity.^[75] Generally, metal hydroxides can be prepared from MOF templates through two common methods including alkaline hydrolysis and etching.^[76] For the alkaline method, MOFs undergo hydrolysis under alkaline conditions, and the organic ligands are substituted by OH⁻ ions to form metal hydroxides. Jiang et al reported the synthesis of 3D hierarchical NiCo-LDH microspheres through a simple and gentle alkaline hydrolysis method by immersing NiCo-MOF precursors in NaOH solution at room temperature for 2 h.^[77] Benefiting from the hierarchical structure facilitating charge transfer, the resulting electrode exhibited high activity (1750.0 F g⁻¹ at 1 A g⁻¹). The etching strategy represents another popular approach for constructing metal hydroxides from MOFs, particularly ZIFs. During the synthesis, protons are first generated from the hydrolysis of metal ions, which etches ZIF gradually to release metal ions. The co-precipitation of metal

ions with OH⁻ produces metal hydroxides.^[78] Hollow structures are usually obtained through this method due to the Kirkendall effect, which is conducive to ion diffusion and excellent electrochemical performance.^[79,80] Yang et al. synthesized MnCoNi-LDH by a simple one-pot hydrothermal method using ZIF-67 as the template.^[51] The prepared MnCoNi-LDH presented a distinctive polyhedral hollow structure, thereby resulting in excellent specific capacity (2254 F g⁻¹ at 1 A g⁻¹). The assembled MnCoNi-LDH//AC ASC delivered a high energy density of 47.42 Wh kg⁻¹ at a power density of 404.1 W kg⁻¹. Despite these advances, powdery electrode materials need to be blended with insulating polymer binders and conductive additives to prepare the electrode, resulting in interfacial resistance and "dead volume". To overcome this issue, it is ideal to deposit MOF-derived architectures on conductive substrates directly. For example, Zheng et al. constructed a distinctive hierarchical core/shell homogeneous structure with NiCo-LDH nanorods (NCNRs) as cores and NiCo-LDH nanosheets (NCNSs) as shells through an in situ ZIF shell growth and ion exchange-coprecipitation process, as demonstrated in Figure 6a.^[52] The NCNRs evenly covered on the NF (Figure 6b, c) were partially converted into ZIF intermediates (Figure 6d, e) in 2-methylimidazole (MIM) solution. In presence of Ni (NO₃)₂·6H₂O, the ZIF precursors were transformed into NCNSs (Figure 6f, g) through the typical etching and coprecipitation mechanism. The prepared NCNRs@NCNSs electrode showed a very high specific capacitance of 2640.2 F g⁻¹ at 1 A g⁻¹. The ASC assembled

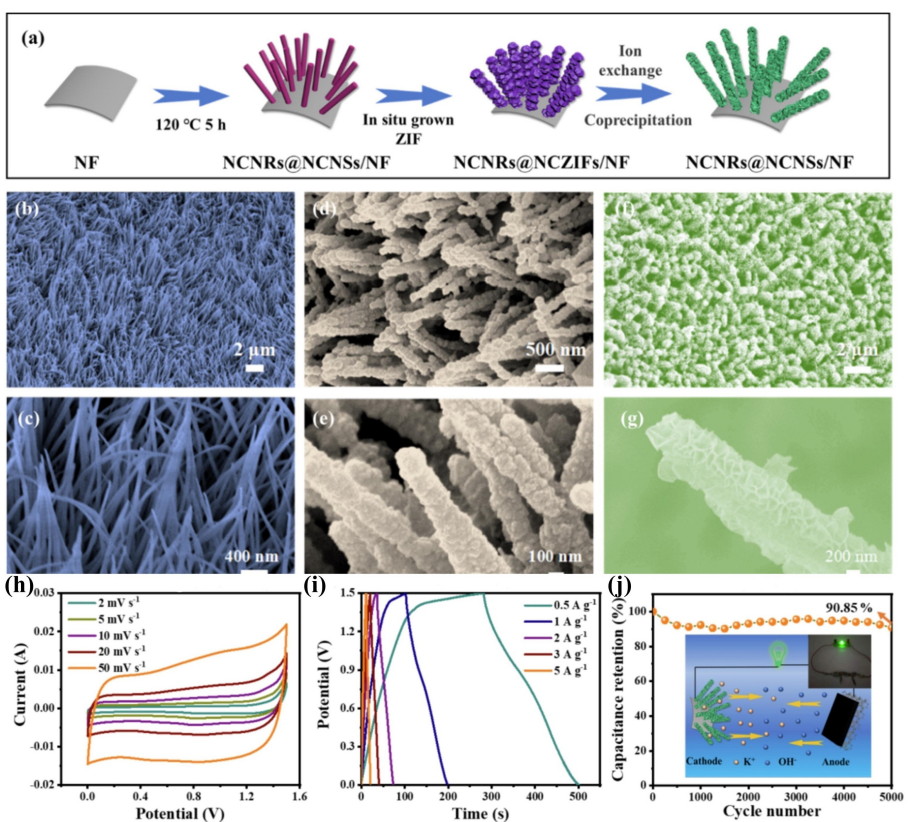


Figure 6. (a) Schematic illustration of the synthesis of the NCNRs@NCNSs. The SEM images of (b, c) NCNRs, (d, e) NCNRs@NCZIFs and (f, g) NCNRs@NCNSs. (h) CV, (i) GCD curves and (j) Cycling performance of the assembled NCNRs@NCNSs//AC. The inset in (j) shows a green LED assembly schematic diagram and physical diagram after lighting, Reprinted with permission from ref. [52], Copyright 2022, Elsevier.

NCNRs@NCNSs//AC ASC possessed good electrochemical performance (Figure 6h, i), displaying an energy density of 22.81 Wh kg^{-1} with 374.95 W kg^{-1} . Besides, the ASC device could retain 90.85% capacitance after 5000 cycles. The hierarchical structure could provide rich active sites for redox reactions, and the freestanding configuration ensured robust structure.

Recently, transition metal sulfides (TMSs) and their composites have attracted much attention in ASCs in view of their excellent properties such as high specific capacity, and improved conductivity in contrast to metal oxide/hydroxide counterparts.^[18,81] MOF has been proved to be an ideal precursor/template to prepare porous/hollow TMSs-based micro-nanostructures, which shows improved electrochemical performance.^[82] Chen et al. designed a hollow structure of NiCo_2S_4 spheres with rich sulfur vacancies (r- NiCo_2S_4) through ligand exchange reaction, sulfidation and simple reduction using ZIF-67 as the precursor (Figure 7a).^[53] The hollow structure could provide rich electroactive sites for redox reactions, and the introduction of S vacancies resulted in modified electronic conductivity and charge transfer. Therefore, the r- NiCo_2S_4 demonstrated to be an ideal electrode material for SCs. The r- NiCo_2S_4 //AC ASC presented an excellent energy density of 43.8 Wh kg^{-1} at 800 W kg^{-1} with decent cycling performance (93.9% after 10,000 cycles). In another work, Velayutham et al. prepared iron-molybdenum sulfide on nickel foam (denoted as Fe- MoS_2 @NF) using Fe-MOF as the precursor, as shown in Figure 7b.^[54] The synthesized electrode presented palm flower like nanostructure and provided a high areal capacity of

3565 mC cm^{-2} at 4 mA cm^{-2} . An ASC was prepared by using Fe- MoS_2 @NF as the positive electrode and O, N, and S@AC as the negative electrode. The prepared ASC exhibited provided an energy density of 49.4 Wh kg^{-1} at a power density of 827 W kg^{-1} with excellent cycling stability (91% after 10,000 cycles). Kang and coworkers prepared hollow rod-like NiCoMn ternary metal sulfide nanosheets through etching/ion-exchange reaction and additional vulcanization using ZIF-67 as the precursor.^[55] The NiCoMn-S nanosheet exhibited a high specific capacitance of 2098.2 F g^{-1} at 1 A g^{-1} , originating from the unique hierarchical structure and synergy among Ni/Co/Mn ions. The NiCoMn-S//AC displayed a maximum energy density of 50.0 Wh kg^{-1} .

Transition metal phosphides, as an emerging and prominent electroactive materials, have attracted much attention in the field of energy storage owing to their high conductivity and metal-like properties.^[83] For example, Chu et al. synthesized a zinc-cobalt phosphide electrode with excellent electrical conductivity from MOF template (Figure 8a).^[56] The ZnCo-MOF precursors were transformed ZnCo_2O_4 after annealing in air. Following a phosphatization in inert atmosphere, the phosphorus ions were exchanged with oxygen ions to produce ZnCoP. The theoretical calculation revealed that the incorporation of P resulted in a narrowed band gap, thereby enhancing the electrical conductivity. Therefore, the obtained electrode displayed high specific capacitance (2115.5 F g^{-1} at 1 A g^{-1}) and excellent rate performance (51% at 50 A g^{-1}). The fabricated $\text{Zn}_{0.33}\text{Co}_{0.67} \text{P}/\text{Bi}_2\text{O}_3$ ASC delivered a high-energy intensity of 83.05 Wh kg^{-1} at a power density of 775.02 W kg^{-1} . In another

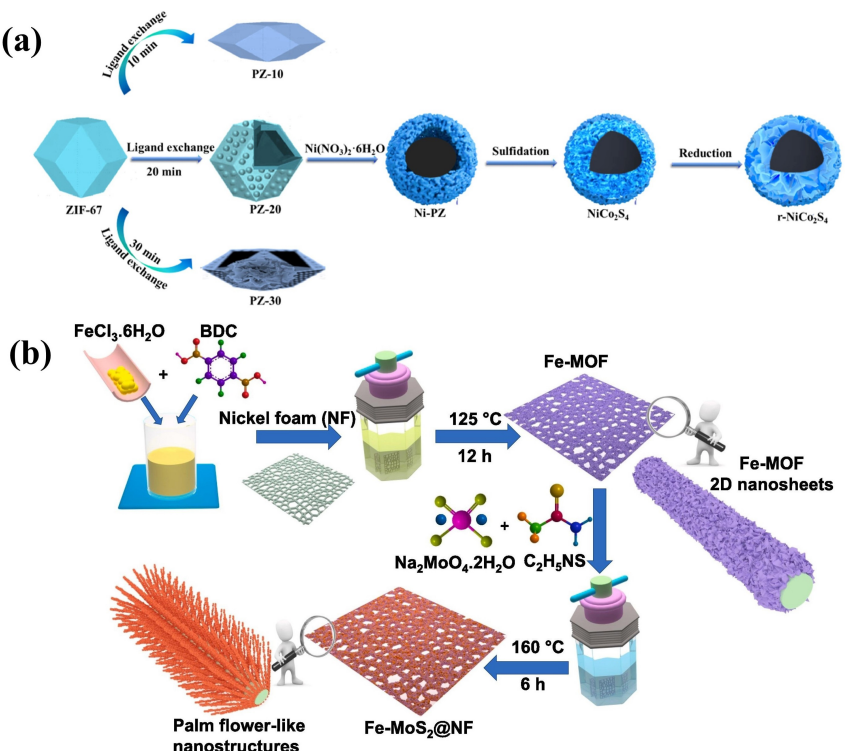


Figure 7. (a) Schematic illustration of the preparation of r- NiCo_2S_4 . Reprinted with permission from ref. [53], Copyright 2022, Elsevier. (b) Schematic illustration for the synthesis of Fe- MoS_2 @NF electrode. Reprinted with permission from ref. [54], Copyright 2021, Elsevier.

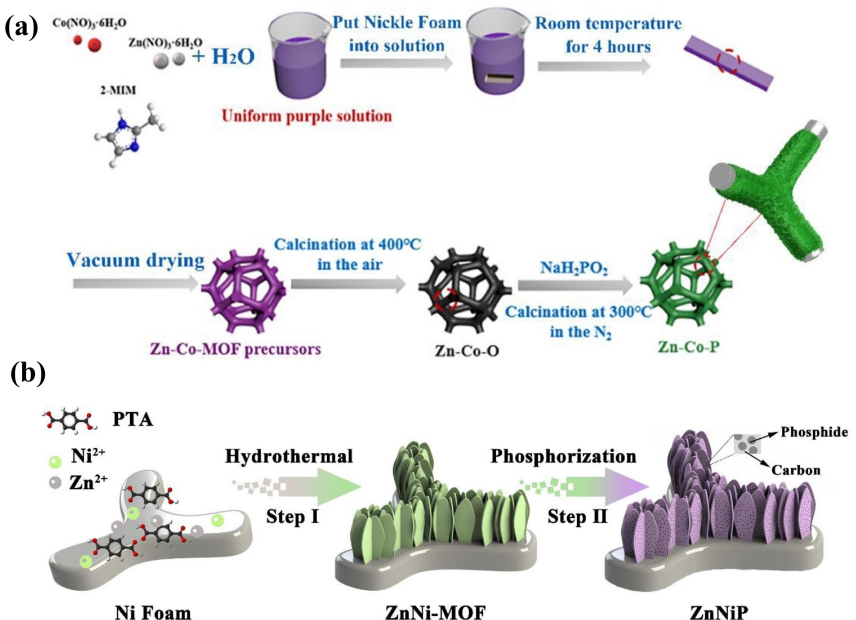


Figure 8. (a) Schematic illustration of the fabrication process of the ZnCoP. Reprinted with permission from ref. [56], Copyright 2020, Elsevier. (b) Schematic illustration of the synthetic of ZnNiP nanosheet arrays. Reprinted with permission from ref. [57], Copyright 2021, Elsevier.

work, Yang et al. prepared a binder-free ZnNiP electrode by direct phosphatization of Zn-doped Ni-MOF (Figure 8b).^[57] It is noteworthy that the incorporation of the Zn sources and the phosphorylation process allowed the components to act synergistically to improve the electrical conductivity, and enriched the electroactive sites. When the ZnNiP electrode was coupled with reduced graphene oxide (rGO), the obtained ASC could output a maximum energy density of 67.4 Wh kg^{-1} and a maximum power density of 15.9 kW kg^{-1} . Wang's team prepared S, C co-doped trimetallic phosphide nanorods based on high valence metal-engineered thiophene-based MOF.^[84] Taking the advantages of electronic coupling of multiple interfaces and the synergy of components, the prepared SC-FeNiCeP/NF nano-arrays achieved a high specific capacitance of 2290 F g^{-1} at 1 A g^{-1} .

Nowadays, other transition metal compounds based on MOFs are also explored as positive electrodes for ASCs. For example, Zhang et al. reported the preparation of Ni–Fe–Mn–Se nanoboxes with a bilayer hollow structure using NiFe Prussian blue analog (NiFe-PBA) as the template.^[58] The combination of polymetallic elements with selenium effectively modulated the electronic structure of the material, thereby improving the electrical conductivity. Therefore, the Ni–Fe–Mn–Se exhibited a high specific capacitance of 1433 F g^{-1} at 1 A g^{-1} . The Ni–Fe–Mn–Se//AC demonstrated a maximum energy density of 66.8 Wh kg^{-1} at a power density of 791 W kg^{-1} . A polypyrrole (PPy) wrapped CoFe-PBA was synthesized by Ding et al., and the nitrogen-doped carbon (NC) coated with (CoFe)Se₂ was obtained by one-step selenization of the CoFe-PBA@PPy precursor.^[59] Benefiting from the robust porous structure and high conductivity of NC, the (CoFe)Se₂@NC exhibited excellent electrochemical performance as a positive electrode for ASC. It delivered a high specific capacitance of

867 F g^{-1} at 1 A g^{-1} . More importantly, it maintained 99% initial capacitance after 20,000 cycles at 5 A g^{-1} , showing a clear advantage compared to the electrodes made up of similar metal selenides. Zhang et al. achieved the conversion of ZIF-67 to CoSe₂ by a simple selenization method, after which wire-sheet-particle layered heterostructured electrodes consisting of 1D CuBr₂, 2D NiMn-LDH and 3D CoSe₂ were used for ASC.^[85] With CoSe₂@NiMn-LDH@Cu_{1.8}Se/CF as the positive electrode and AC as the negative electrode, the assembled ASC device delivered an energy density of 36.6 Wh kg^{-1} at a power density of 760.6 W kg^{-1} .

A great deal of research has been carried out by exploring MOFs as positive electrode materials for ASCs, since the multiple oxidation states of metal ions enable rich redox reactions and high capacity. To overcome the poor electronic conductivity and instability of pristine MOFs, it is ideal to couple MOFs with conductive substances to make composites, or design conductive MOFs through coordination chemistry. In another way, MOFs can be converted into metal compounds including metal oxides/hydroxides, metal sulfides, metal phosphides, and metal selenides through proper treatments. The MOF derivatives usually featured by porous and hollow microstructures, thereby demonstrate high specific capacitance in three-electrode system. However, further optimization of the electrochemical performance including cycle life and device performance of the assembled ASC is still needed.

2.3. Negative and Positive Electrodes

For ASCs, the negative and positive electrodes are usually quite different. The similar structure of the two electrodes is more favorable for the migration of electrons between the two

electrodes. Designing two electrodes from the same MOF precursor known as “one for two” strategy has attracted great interest due to the ease synthesis and low cost.^[60] For example, a novel iron-based MOF Fe(TATB)(Tipa)(H₂O) (FeSC) with 3D interpenetrated structure was successfully prepared through a hydrothermal method reported by Wang et al.^[60] By heating FeSC at high temperature, a Fe₂O₃/Fe₃N/Fe₃C (FeSC#) composite was obtained. FeSC and FeSC# acted as positive and negative electrode materials to assemble an ASC (Fe-ASC), which could output a high energy density of 49.85 Wh kg⁻¹. Porous carbon nanofibers (CNF) embedded with N-doped porous carbon (NPC) nanoparticles and ZnO quantum dots (ZnO QDs) were prepared by Li et al. through co-electrospinning of ZIF-8 and PAN followed by carbonization.^[61] The embedding of NPC nanoparticles increased the specific surface area and conductivity of the CNFs, and stabilized the mechanical structure, while the incorporation of ZnO QDs provided abundant active sites. Consequently, the ZnO QD/NPC/CNF electrode exhibited a high specific capacity of 71.6 mAh g⁻¹ (644.4 Fg⁻¹) at 1 A g⁻¹. The NPC/CNF was simply prepared by acid etching. The ZnO QD/NPC/CNF and NPC/CNF were used as positive and negative electrodes to assemble an ASC, which delivered an energy density of 33.8 Wh kg⁻¹ at a power density of 800 W kg⁻¹. He et al. synthesized nanoporous carbon (NPC) and porous bimetallic oxides (ZnCo₂O₄) from the same bimetallic Zn/Co-MOF template (Figure 9a), and the MOF-derived NPC and ZnCo₂O₄ were as positive and negative materials to assemble an ASC device.^[62] Bimetallic Zn/Co-MOF polyhedrons were first obtained through co-precipitation of Zn²⁺, Co²⁺ and 2-MIM at room temperature. Following a pyrolysis at 900 °C and acid etching, NPC was obtained. The ZnCo₂O₄ was prepared by direct annealing of Zn/Co-MOF in air. Both NPC and ZnCo₂O₄ electrode materials exhibited hierarchical porous structures with large specific surface areas and appropriate mesopore-to-

microporous ratios, which not only provided rich active sites for redox reaction, but also offered channels for fast ions diffusion. The assembled ASC displayed excellent energy storage performance with a high specific capacitance of 94.4 F g⁻¹ (cell) and a maximum energy density of 28.6 Wh kg⁻¹ at a power density of 100 W kg⁻¹ (Figure 9b, c).

The two electrodes of ASCs can be prepared from same type of MOF but with different metal nodes. For instance, Dong et al. successfully prepared isomorphic MOFs of Co-TAMBA and Fe-TAMBA using a novel azole carboxylic acid ligand and converted them into two derivatives of Co-TAMBA-d and Fe-TAMBA-d by calcination under N₂ atmosphere.^[63] The ASC assembled with Co-TAMBA-d as positive electrode and Fe-TAMBA-d as negative electrode showed excellent electrochemical performance with an energy density of 47 Wh kg⁻¹ at a power density of 1658 W kg⁻¹. The two electrodes of ASCs can also be prepared by using two different types of MOFs as the precursors. Poudel et al. prepared a positive electrode by anchoring MOF-derived ZnNiCo-LDH nanosheets on copper oxide (Cu_xO) nanowire arrays in-situ-grown on Cu foam, and a negative electrode N-CNT by pyrolysis of Co-MOF followed by acid etching.^[64] Vertically aligned ZnNiCo-LDH nanosheets adhered on conductive CuO nanowire arrays contributed to large active sites and fast charge transfer. As a result, the ZnNiCo-LDH/CuO-Cu exhibited high specific capacity (378.10 mAh g⁻¹ at 1 A g⁻¹). The fabricated ZnNiCo-LDH/CuO-Cu/N-CNT ASC could deliver a high specific energy density of 117.5 Wh kg⁻¹ at a power density of 576.9 W kg⁻¹. Moreover, the specific capacity was maintained stable during 10,000 charge/discharge cycles. POMOFs featured by abundant redox-active sites and ordered structures are also employed to construct ASCs. Liu et al. reported a POMOF-based ASC by using NENU-5/PPy as the positive electrode and PMo₁₂@MIL-101-derived FeMo/C as the negative electrode.^[65] The positive

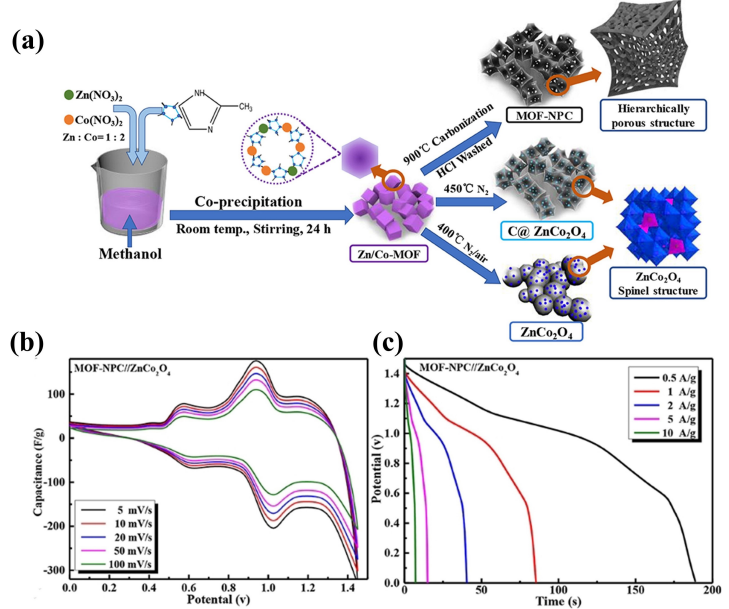


Figure 9. (a) Schematic illustration for the synthesis of Zn/Co-MOF-derived NPC and ZnCo₂O₄. (b) CV and (c) GCD curves of the assembled NPC//ZnCo₂O₄. Reprinted with permission from ref. [62], Copyright 2020, Frontiers.

electrode could provide high capacitance, while the negative electrode could exhibit outstanding cycling stability. As a result, the assembled ASC could achieve an energy density of 1.12 mWhcm^{-3} at a power density of 27.78 mWcm^{-3} . In addition, it retained 80.62% initial capacitance after 10,000 cycles.

The application of MOF-based materials for both negative and positive electrodes is particularly attractive in ASCs. Positive and negative electrodes from the same or similar MOF-based precursors can largely simplify the synthesis process, and in some cases the prepared ASCs have excellent electrochemical properties. However, there is still room for exploring other MOF-based electrode materials to further improve the energy storage properties.

3. Summary and Future Outlook

This paper summarizes recent advances in ASCs based on MOF-based electrode materials including pristine MOFs, MOF derivatives and their composites. Benefiting from high porosity and rich electroactive sites, MOF and its derivatives present excellent electrochemical performance when used as negative electrode, positive electrode or both, which provides a great opportunity to fabricate ASCs with the required high energy/power density. However, there are still some challenges in MOF-based ASCs. Firstly, the applications of pristine MOFs are still restricted by their intrinsic low conductivity and instability in electrolytes. It is desirable to couple MOFs with conductive substances to make composites, or design conductive MOFs through coordination chemistry. Secondly, although MOF derivatives retain the shape and porous structure in some extent, the powdery electrode materials need to be blended with insulating polymer binders and conductive additives to prepare the electrode, resulting in interfacial resistance and "dead volume". It is ideal to construct MOF-based arrays on conductive substances directly. The MOF derivatives usually possess porous and hollow structure, which increases the exposed electrochemically active sites. However, the electronic structure is not modulated. Recent studies suggest that the electronic structure and the surface chemical properties of active materials can be optimized through defect engineering, thereby improving the electrochemical performance. Lastly but not least, MOF-based electrode materials usually exhibit high electrochemical activity in three-electrode systems, but the assembled ASCs display moderate energy density, since most of the negative electrode materials of are still carbon materials. It is imperative to develop high-performance negative materials. The "one for two" strategy by preparing two electrodes both from MOF precursors will simplify the synthesis. Further optimizing charge matching between two electrodes is required to achieve boosted energy storage properties of ASCs.

Acknowledgements

The financial support from the Natural Science Foundation of Ningbo (2022J094) is greatly appreciated.

Conflict of Interests

The authors declare no competing financial interest.

Keywords: Asymmetric supercapacitors • Metal-organic framework • Electrode materials

- [1] X. Luo, R. Abazari, M. Tahir, W. K. Fan, A. Kumar, T. Kalhorizadeh, A. M. Kirillov, A. R. Amani-Ghadim, J. Chen, Y. Zhou, *Coord. Chem. Rev.* **2022**, *461*, 214505.
- [2] K.-B. Wang, Q. Xun, Q. Zhang, *EnergyChem* **2020**, *2* (1), 100025.
- [3] H. Cheng, J. Li, T. Meng, D. Shu, *Small* **2024**, *20* (20), 2308804.
- [4] F. Zhan, S. Liu, Q. He, X. Zhao, H. Wang, M. Han, Y. Yamauchi, L. Chen, *Energy Storage Mater.* **2022**, *52*, 685–735.
- [5] A. T. Zhang, K. Wang, M.. J. Nine, M. Y. Cao, H. W. Zong, Z. Q. Liu, H. W. Guo, J. Q. Liu, D. Losic, *Green Energy & Environ.* **2024**, *9* (2), 378–389.
- [6] Y. Guo, J. Bae, Z. Fang, P. Li, F. Zhao, G. Yu, *Chem. Rev.* **2020**, *120* (15), 7642–7707.
- [7] K. Mathiyalagan, D. Shin, Y.-C. Lee, *J. Energy Chem.* **2024**, *90*, 40–57.
- [8] C.-F. Liu, Y.-C. Liu, T.-Y. Yi, C.-C. Hu, *Carbon* **2019**, *145*, 529–548.
- [9] G. Kothandam, G. Singh, X. Guan, J. M. Lee, K. Ramadass, S. Joseph, M. Benzigar, A. Karakoti, J. Yi, P. Kumar, A. Vinu, *Adv. Sci. (Weinh)* **2023**, *10* (18), 2301045.
- [10] C. Li, H. Yan, H. Yang, M. Yue, S. Li, K. Wang, *Batteries & Supercaps* **2024**, *7* (9), e202400193.
- [11] P. A. Shinde, Q. Abbas, N. R. Chodankar, K. Ariga, M. A. Abdelkareem, A. G. Olabi, *J. Energy Chem.* **2023**, *79*, 611–638.
- [12] D. P. Chatterjee, A. K. Nandi, *J. Mater. Chem. A* **2021**, *9* (29), 15880–15918.
- [13] K. O. Oyedotun, J. O. Ighalo, J. F. Amaku, C. Olisah, A. O. Adeola, K. O. Iwuozior, K. G. Akpomie, J. Conradie, K. A. Adegoke, *J. Electron. Mater.* **2022**, *52* (1), 96–129.
- [14] A. Zhang, Q. Zhang, H. Fu, H. Zong, H. Guo, *Small* **2023**, *19* (48), 2303911.
- [15] Z.-X. Wu, L.-Q. Fan, J.-J. Chen, X.-G. Deng, T. Tang, Y.-F. Huang, J.-H. Wu, *J. Colloid Interface Sci.* **2023**, *649*, 880–889.
- [16] N. Choudhary, C. Li, J. Moore, N. Nagaiah, L. Zhai, Y. Jung, J. Thomas, *Adv. Mater.* **2017**, *29* (21), 1605336.
- [17] M. Qorbani, K.-H. Chen, L.-C. Chen, *Small* **2024**, *20* (33), 2400558.
- [18] Y. Gao, L. Zhao, *Chem. Eng. J.* **2022**, *430*, 132745.
- [19] N. Wu, X. Bai, D. Pan, B. Dong, R. Wei, N. Naik, R. R. Patil, Z. Guo, *Adv. Mater. Interfaces* **2021**, *8* (1), 2001710.
- [20] Y. Shao, M. F. El-Kady, J. Sun, Y. Li, Q. Zhang, M. Zhu, H. Wang, B. Dunn, R. B. Kaner, *Chem. Rev.* **2018**, *118* (18), 9233–9280.
- [21] P. O. Anikpa, A. U. Mee, A. C. Nwanya, A. C. Nkele, D. B. Malavekar, R. U. Osuji, N. Nwulu, C. D. Lokhande, F. I. Ezema, *J. Storage Mater.* **2024**, *81*, 110439.
- [22] C. Qu, Z. Liang, Y. Jiao, B. Zhao, B. Zhu, D. Dang, S. Dai, Y. Chen, R. Zou, M. Liu, *Small* **2018**, *14* (23), 1800285.
- [23] H. L. Wang, W. W. Jiang, S. Chen, J. F. Chen, F. Wu, R. Liang, *Chem. Eng. J.* **2023**, *474*, 145755.
- [24] W. Du, Y.-L. Bai, J. Xu, H. Zhao, L. Zhang, X. Li, J. Zhang, *J. Power Sources* **2018**, *402*, 281–295.
- [25] Y. Cao, W. Yang, M. Wang, N. Wu, L. Zhang, Q. Guan, H. Guo, *Int. J. Hydrogen Energy* **2021**, *46* (35), 18179–18206.
- [26] D. Tian, N. Song, M. Zhong, X. Lu, C. Wang, *ACS Appl. Mater. Interfaces* **2019**, *12* (1), 1280–1291.
- [27] S. Wang, Y.-z. Guo, F.-x. Wang, S.-h. Zhou, T.-y. Zeng, Y.-b. Dong, *New Carbon. Mater.* **2022**, *37* (1), 109–135.
- [28] Q. Liu, R. Li, J. Li, B. Zheng, S. Song, L. Chen, T. Li, Y. Ma, *Chem. A Eur. J.* **2024**, *30* (30), e202400157.
- [29] T. Mehtab, G. Yasin, M. Arif, M. Shakeel, R. M. Korai, M. Nadeem, N. Muhammad, X. Lu, *J. Storage Mater.* **2019**, *21*, 632–646.
- [30] X. Li, X. Yang, H. Xue, H. Pang, Q. Xu, *EnergyChem* **2020**, *2* (2), 100027.

- [31] A. Zhang, Q. Zhang, J. Huang, H. Fu, H. Zong, H. Guo, *Chem. Eng. J.* **2024**, *487*, 150587.
- [32] M. Prajapati, V. Singh, M. V. Jacob, C. Ravi Kant, *Renewable Sustainable Energy Rev.* **2023**, *183*, 113509.
- [33] W. Zhao, Y. Zeng, Y. Zhao, X. Wu, *J. Storage Mater.* **2023**, *62*, 106934.
- [34] X. Zhao, K. Tao, L. Han, *Nanoscale* **2022**, *14* (6), 2155–2166.
- [35] B. Xu, H. Zhang, H. Mei, D. Sun, *Coord. Chem. Rev.* **2020**, *420*, 213438.
- [36] Z. Ding, Z. Cheng, N. Shi, Z. Guo, Y. Ren, M. Han, M. Chen, L. Xie, W. Huang, *Chem. Eng. J.* **2022**, *450*, 137193.
- [37] Y. Wang, W. Lu, L. Wang, Y. Li, H. Wu, X. Zhu, C. Zhang, K. Wang, *Nanotechnology* **2024**, *35* (20), 205402.
- [38] T. Kim, S. Subedi, B. Dahal, K. Chhetri, T. Mukhiya, A. Muthurasu, J. Gautam, P. C. Lohani, D. Acharya, I. Pathak, S.-H. Chae, T. H. Ko, H. Y. Kim, *Adv. Sci.* **2022**, *9* (20), 2200650.
- [39] M. S. Javed, N. Shaheen, S. Hussain, J. Li, S. S. A. Shah, Y. Abbas, M. A. Ahmad, R. Raza, W. Mai, *J. Mater. Chem. A* **2019**, *7* (3), 946–957.
- [40] M. S. Javed, M. K. Aslam, S. Asim, S. Batool, M. Idrees, S. Hussain, S. S. A. Shah, M. Saleem, W. Mai, C. Hu, *Electrochim. Acta* **2020**, *349*, 136384.
- [41] S. Xiong, X. Lin, S. Liu, S. Weng, S. Jiang, Y. Jiao, Y. Xu, J. Cheng, *Vacuum* **2020**, *182*, 109692.
- [42] L. Sun, Y. Cai, M. K. Haider, D. Miyagi, C. Zhu, I. S. Kim, *Composites Part B* **2022**, *236*, 109812.
- [43] J. Wang, W. Wang, H. Wang, W. Zhang, Y. Zhen, F. Fu, B. Xu, *Inorg. Chem. Front.* **2023**, *10* (20), 5969–5978.
- [44] S. Nagamuthu, K.-S. Ryu, *CrystEngComm* **2019**, *21* (9), 1442–1451.
- [45] Q. Liu, Z. Guo, C. Wang, S. Guo, Z. Xu, C. Hu, Y. Liu, Y. Wang, J. He, W. Y. Wong, *Adv. Sci. (Weinh)* **2023**, *10* (18), 2207545.
- [46] M. Reddy Pallavolu, A. Narayan Banerjee, N. Roy, D. Merum, J. Nallapurreddy, S. Woo Joo, *Chem. Eng. J.* **2024**, *498*, e202400157.
- [47] L. Yue, L. Chen, X. Wang, D. Lu, W. Zhou, D. Shen, Q. Yang, S. Xiao, Y. Li, *Chem. Eng. J.* **2023**, *451*, 138687.
- [48] G. Wang, Z. Yan, N. Wang, M. Xiang, Z. Xu, *ACS Appl. Nano Mater.* **2021**, *4* (9), 9034–9043.
- [49] L. Wang, Y. Jiao, S. Yao, P. Li, R. Wang, G. Chen, *Inorg. Chem. Front.* **2019**, *6* (6), 1553–1560.
- [50] A. D. Salunkhe, P. S. Pawar, P. K. Pagare, A. N. Kadam, P. K. Katkar, A. P. Torane, *J. Electroanal. Chem.* **2023**, *939*, 117475.
- [51] H. Yang, Y. Sun, C. Wang, Y. Li, M. Wei, *J. Electroanal. Chem.* **2023**, *928*, 117051.
- [52] K. Zheng, L. Liao, Y. Zhang, H. Tan, J. Liu, C. Li, D. Jia, *J. Colloid Interface Sci.* **2022**, *619*, 75–83.
- [53] Y. Chen, H. Guo, F. Yang, N. Wu, Z. Pan, B. Liu, M. Wang, J. Xu, W. Yang, *Electrochim. Acta* **2022**, *434*, 141319.
- [54] R. Velayutham, R. Manikandan, C. Justin Raj, A. Dennynson Savariraj, W.-J. Cho, H.-M. Jang, B. Chul Kim, *Appl. Surf. Sci.* **2021**, *570*, 151051.
- [55] C. Kang, L. Ma, Y. Chen, L. Fu, Q. Hu, C. Zhou, Q. Liu, *Chem. Eng. J.* **2022**, *427*, 131003.
- [56] W. Chu, Y. Hou, J. Liu, X. Bai, Y. Gao, *Electrochim. Acta* **2020**, *364*, 137063.
- [57] Y. Yang, S. Li, W. Huang, S. Duan, P. Si, L. Ci, *Electrochim. Acta* **2021**, *387*, 138548.
- [58] C. Zhang, Q. Sui, L. Lu, Y. Zou, F. Xu, L. Sun, C. Xiang, *J. Storage Mater.* **2023**, *68*, 107711.
- [59] H. Ding, S. Zhao, X. Wang, C. Qian, T. Zou, X. Li, H. Li, F. Jiang, Y. Liu, H. Cao, Z. Fang, Y. Zhu, *Colloids Surf. A* **2023**, *668*, 131462.
- [60] S. Wang, S. Wang, X. Guo, Z. Wang, F. Mao, L. Su, H. Wu, K. Wang, Q. Zhang, *Inorg. Chem. Front.* **2021**, *8* (22), 4878–4886.
- [61] Z. Li, J. Bu, C. Zhang, L. Cheng, D. Pan, Z. Chen, M. Wu, *New J. Chem.* **2021**, *45* (24), 10672–10682.
- [62] X. Wang, X. Li, C. Huang, C. Hao, C. Ge, Y. Guo, *Appl. Surf. Sci.* **2020**, *527*, 146891.
- [63] Y. Dong, J. Liu, H. Zhang, Q. Li, F. Mao, A. Lu, H. Wu, K. Wang, C. Zhang, Q. Zhang, *SmartMat* **2023**, *4* (3), e1159.
- [64] M. B. Poudel, P. C. Lohani, D. Acharya, D. R. Kandel, A. A. Kim, D. J. Yoo, *J. Storage Mater.* **2023**, *72*, 108220.
- [65] Y.-Z. Liu, W. Yao, H.-M. Gan, C.-Y. Sun, Z.-M. Su, X.-L. Wang, *Chem. A Eur. J.* **2019**, *25* (72), 16617–16624.
- [66] K. Makgopa, M. S. Ratsoma, K. D. Modibane, *Curr. Opin. Electrochem.* **2022**, *36*, 101112.
- [67] C. Li, C. Yan, Q. Yang, P. Huo, *Electrochim. Acta* **2024**, *478*, 143835.
- [68] S. C. Kim, S. Q. Choi, J. Park, *Nanomaterials* **2023**, *13* (12), 1824.
- [69] Z. Wang, X. Mao, P. Chen, M. Xiao, S. A. Monny, S. Wang, M. Konarova, A. Du, L. Wang, *Angew. Chem. Int. Ed.* **2018**, *58* (4), 1030–1034.
- [70] S. Zhang, X. Wang, Y. Li, Y. Zhang, Q. Hu, X. Hua, G. Liu, E. Xie, Z. Zhang, *J. Colloid Interface Sci.* **2020**, *565*, 458–464.
- [71] J. Pan, H. Sun, X. Yan, W. Zhong, W. Shen, Y. Zhang, X. Cheng, *Ceram. Int.* **2020**, *46* (16), 24805–24815.
- [72] A. Shahzad, F. Ahmad, S. Atiq, M. Saleem, O. Munir, M. A. Khan, S. M. B. Arif, Q. U. Ain, S. Sarwar, M. Asim, U. Habib, *J. Storage Mater.* **2024**, *87*, 111447.
- [73] H. Yang, Y. Liu, X. Sun, H. Zhang, C. Zhu, X. Yin, Z. Li, X. Ma, *J. Alloys Compd.* **2022**, *903*, 163993.
- [74] R. Ramachandran, Y. Lan, Z.-X. Xu, F. Wang, *ACS Appl. Energ. Mater.* **2020**, *3* (7), 6633–6643.
- [75] M. Prajapati, C. Ravi Kant, M. V. Jacob, *J. Electroanal. Chem.* **2024**, *961*, 118242.
- [76] F. Luo, X. San, Y. Wang, D. Meng, K. Tao, *Dalton Trans.* **2024**, *53* (25), 10403–10415.
- [77] D. Jiang, C.-Y. Wei, Z.-Y. Zhu, X.-H. Guan, M. Lu, X.-J. Zhang, G.-S. Wang, *Inorg. Chem. Front.* **2021**, *8* (19), 4324–4333.
- [78] X. Cao, C. Tan, M. Sindoro, H. Zhang, *Chem. Soc. Rev.* **2017**, *46* (10), 2660–2677.
- [79] X. Liu, S. Ding, L. Ye, Y. Du, L. Zhao, Y. Zhu, *Chem. Eng. J.* **2020**, *399*, 125789.
- [80] Y. Du, G. Li, M. Chen, X. Yang, L. Ye, X. Liu, L. Zhao, *Chem. Eng. J.* **2019**, *378*, 122210.
- [81] S. E. Moosavifard, A. Mohammadi, M. Ebrahimnejad Darzi, A. Kariman, M. M. Abdi, G. Karimi, *Chem. Eng. J.* **2021**, *415*, 128662.
- [82] M. I. da Silva, I. R. Machado, H. E. Toma, K. Araki, L. Angnes, J. M. Gonçalves, *J. Mater. Chem. A* **2022**, *10* (2), 430–474.
- [83] X. Zhang, J. Wang, Y. Sui, F. Wei, J. Qi, Q. Meng, Y. He, D. Zhuang, *ACS Appl. Nano Mater.* **2020**, *3* (12), 11945–11954.
- [84] Q. Wang, X. Ma, W. You, P. Ma, R. Bi, S. Song, F. Chen, F. Qu, X. Wang, P. Liu, *Chem. Eng. J.* **2024**, *482*, 148712.
- [85] Q. Zhang, S. Liu, J. Huang, H. Fu, Q. Fan, H. Zong, H. Guo, A. Zhang, *J. Colloid Interface Sci.* **2024**, *655*, 273–285.
- [86] C. Guan, W. Zhao, Y. Hu, Z. Lai, X. Li, S. Sun, H. Zhang, A. K. Cheetham, J. Wang, *Nanoscale Horiz.* **2017**, *2* (2), 99–105.

Manuscript received: August 7, 2024

Revised manuscript received: November 13, 2024

Accepted manuscript online: November 18, 2024

Version of record online: November 27, 2024